arXiv:1210.7725v1 [nucl-th] 29 Oct 2012

Theoretical analysis of $\Lambda(1405) \to (\Sigma\pi)^0$ mass spectra produced in $p + p \to p + \Lambda(1405) + K^+$ reactions

Maryam Hassanvand[1,2], Seyed Zafarollah Kalantari[2], Yoshinori Akaishi[1,3], and Toshimitsu Yamazaki[1,4]
[1] *RIKEN, Nishina Center, Wako, Saitama 351-0198, Japan*
[2] *Department of Physics, Isfahan University of Technology, Isfahan 84156-83111, Iran*
[3] *College of Science and Technology, Nihon University, Funabashi, Chiba 274-8501, Japan and*
[4] *Department of Physics, University of Tokyo, Bunkyo-ku, Tokyo 113-0033, Japan*

We formulated the $\Lambda(1405)$ (abbreviated as Λ^*) $\to (\Sigma\pi)^0$ invariant-mass spectra produced in $p + p \to p + \Lambda^* + K^+$ reactions, in which both the incident channel for a quasi-bound K^-p state and its decay process to $(\Sigma\pi)^0$ were taken into account realistically. We calculated $M(\Sigma\pi)$ spectral shapes for various theoretical models for Λ^*. They are asymmetric and skewed, and were compared with recent experimental data of HADES, yielding $M(\Lambda^*) = 1405^{+11}_{-9}\,\mathrm{MeV}/c^2$ and $\Gamma = 62 \pm 10$ MeV. The nearly isotropic proton distribution observed in DISTO and HADES is ascribed to a short collision length in the production of Λ^*, which justifies the high sticking mechanism of Λ^* and the participating proton into K^-pp.

PACS numbers: 21.45.-v, 13.75.-n, 21.30.Fe, 21.90.+f

I. INTRODUCTION

The $\Lambda(1405)$ resonance discovered in 1961 [1] (called herein Λ^*) has strangeness S = -1, spin-parity $J^p = (\frac{1}{2})^-$ and isospin I=0. It has been interpreted as a quasi-bound state of K^-p embedded in the $\Sigma + \pi$ continuum since Dalitz-Tuan's original prediction [2]. In recent years, Akaishi *et al.* derived phenomenologically a complex $\bar{K}N$ interaction (called here AY interaction) [3–5] based on the mass and width of $\Lambda(1405)$, $M = 1405.1^{+1.3}_{-1.0}$ MeV/c^2 and $\Gamma = 50 \pm 2$ MeV [6–8], (so-called $\Lambda(1405)$ ansatz). They applied this very attractive interaction to few-nucleon systems involving one and two $\bar{K}$'s, and found nuclear bound states with unusually high nuclear density [3, 9–12]. On the other hand, a totally different framework with a double-pole structure of $\Lambda(1405)$ has emerged on the basis of chiral SU(3) dynamics (called here *Chiral*), which claims that $\Lambda(1405)$ consists of two poles around 1420 and 1390 MeV/c^2, which are coupled mainly to $\bar{K}N$ and $\Sigma\pi$ channels, respectively [13, 14]. Then, the resulting weakly attractive $\bar{K}N$ interaction leads to much shallower $\bar{K}$ bound states [15, 16].

Thus, it is vitally important to determine the location of the K^-p resonance, "whether $\Lambda(1405)$ is located at 1405 MeV/c^2 or above 1420 MeV/c^2", from experimental data without prejudice. For this purpose we have to treat the $\Lambda(1405)$ structure with the AY model and the *Chiral* model on equal footing to be compared with experimental data. To solve this issue, observations of $M(\Sigma\pi)$ spectra associated with resonant formation of Λ^* in the stopped-K^- absorption in ^{3,4}He [17], and also in d [18] have been proposed. Whereas old bubble-chamber experiments of stopped K^- in ^{4}He [19] indicated preference of $\Lambda(1405)$ over $\Lambda(1420)$ [8, 18], a much more precise experiment with a deuteron target is expected at J-PARC [20]. Alternatively, Jido *et al.* [21] proposed an in-flight K^- reaction on d, whereas Miyagawa and Haidenbauer [22] questioned about the effectiveness of this method. In any case, old data on the in-flight $K^- + d$ reaction by Braun *et al.* [23] had a large statistical uncertainty in distinguishing $\Lambda(1420)$ and $\Lambda(1405)$, according to our statistical analysis. Future experiments at J-PARC of both stopped-K^- [20] and in-flight K^- [24] on d are expected to give a convincing conclusion.

Recent experiments on high-energy pp collisions have produced important data on the production of $\Lambda(1405)$:

$$\begin{aligned} p + p \to p + \Lambda^* + K^+, \\ \Lambda^* \to \Sigma^{+,0,-} + \pi^{-,0,+}. \end{aligned} \qquad (I.1)$$

The ANKE experiment at COSY with an incident kinetic energy (T_p) of 2.83 GeV by Zychor *et al.* [25] has yielded a $(\Sigma^0\pi^0)^0$ invariant-mass spectrum. It was analyzed by Geng and Oset [26] based on chiral SU(3) dynamics. They showed that the reaction in the Λ^* production region is dominated by the $|T_{21}|^2 q_2$ process, and claimed that the spectrum develops a pronounced strength around 1420 MeV/c^2, which differs from the 1405 MeV/c^2 peak in Hemingway's data [27] analyzed by the $|T_{22}|^2 q_2$ process [6, 7] (see also Akaishi *et al.* [28]). This result might have been accepted as evidence for a double-pole structure of Λ^* predicted by chiral SU(3) dynamics [13, 14], if the statistics of the data were good enough. The ANKE data was also analyzed by Esmaili *et al.* [18], who, on the contrary, showed from a fair statistical comparison between the two models that the data was in more favor of the AY model, but the statistical significance was not sufficient to conclusively distinguish between *Chiral* and AY. Thus, new data from HADES of GSI, which has just been published [29, 30], is valuable for solving the present controversy.

In the present paper we formulate the spectral shape of the $(\Sigma\pi)^0$ mass to provide theoretical guides to analyze experimental data of $(\Sigma\pi)^0$ mass spectra from the above reaction. We take into account both the formation and the decay processes of $\Lambda(1405)$ in pp reactions realistically, following our $\bar{K}N - \Sigma\pi$ coupled-channel formalism method [5]. In this way, we derive the general form of the spectral function, which is not symmetric, but skewed with respect to the pole position. Then, we analyze $(\Sigma^{+-}\pi^{-+})^0$ spectra from HADES at $T_p = 3.50$ GeV [30].

II. FORMULATION

A. Coupled-channel treatment of Λ^*

Our coupled-channel treatment of $\Lambda(1405)$ is described in [5, 18]. The transition matrices of the two coupled channels, $\bar{K}N(1)$ and $\Sigma\pi(2)$, obeys the following equation with a loop function G_l:

$$T_{ij} = U_{ij} + \sum_{l} U_{il} G_l T_{lj}, \tag{II.2}$$

where (i, j)=(1,2) and (2,1). The solution is given in a matrix form by

$$T = [1 - UG]^{-1} U. \tag{II.3}$$

In our treatment, the loop function is considered to be

$$(UG)_{lj} = -s_{lj}\sqrt{\frac{\mu_j}{\mu_l}}\,\frac{\Lambda^2}{(\Lambda - i\,k_j)^2}, \tag{II.4}$$

where k_j is the relative momentum in channel j, and s_{ij}'s are non-dimensional strength parameters [5].

Among the matrix elements, T_{11}, T_{12}, T_{21} and T_{22}, the experimentally observable quantities below the $\bar{K} + N$ threshold are $-(1/\pi)\mathrm{Im}\ T_{11}$, $\mid T_{21} \mid^2\ q_2$ and $\mid T_{22} \mid^2\ q_2$, where the second term is a $\Sigma\pi$ invariant-mass spectrum from the conversion process, $\bar{K}N \rightarrow \Sigma\pi$ (we call this ”T_{21} invariant mass”). The T_{21} invariant mass coincides with the $\bar{K}N$ missing-mass spectrum in the mass region below the $\bar{K} + N$ threshold, as denoted by relation [18], that

$$\mathrm{Im}\, T_{11} = |T_{21}|^2\, \mathrm{Im}\, G_2. \tag{II.5}$$

The third term is a $\Sigma\pi$ invariant-mass spectrum from the scattering process, $\Sigma\pi \longrightarrow \Sigma\pi$ (we call this ”T_{22} invariant mass”).

B. $\Lambda^* \rightarrow (\Sigma\pi)^0$ spectrum shape

The diagram for the reaction eq. (I.1) is shown in Fig. 1. The decay processes via T_{21} and T_{22} are also given in this figure. The kinematical variables in the c.m. of the $p + p$ collision for both the formation and the decay processes are given in Fig. 2.

In the present reaction we use $|T_{21}|^2 q_2$ because the incident channel to bring $\Lambda(1405)$ is $K^- + p$ together with K^+ (see Fig. 1 (b)). This was also concluded by Geng and Oset [26], who studied the reaction mechanism in detail. The $|T_{22}|^2 q_2$ spectrum would be applicable when Σ and π mesons are available in the incident channel, as shown in Fig. 1 (a). The $|T_{22}|^2 q_2$ spectrum is characterized by a large tail [18] in the higher-mass region up to the kinematical limit, which can in principle be recognizable by an observed spectrum. Experimentally, however, a bump in the upper-tail region may be masked by an ambiguous shape of the continuous background, and may thus be difficult to extract. We may allow a small admixture of $|T_{22}|^2 q_2$ in our likelihood analysis of the experimental data.

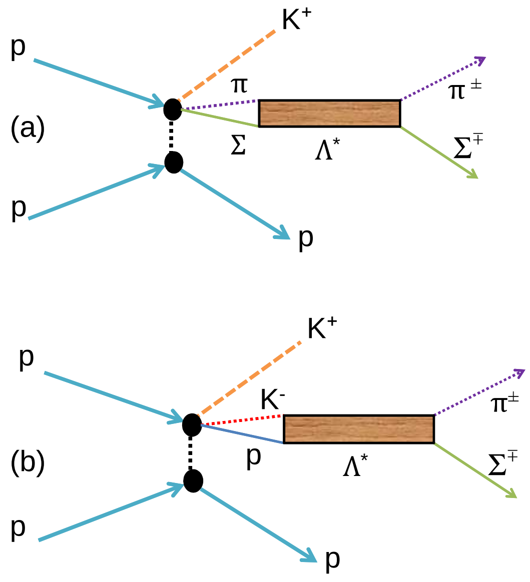

FIG. 1: (Color online) Feynman diagrams for the $p + p \rightarrow p + K^+ + \Lambda^* \rightarrow p + K^+ + (\Sigma\pi)^0$ reaction: (a) for the process via T_{22} and (b) for the process via T_{21}.

The $|T_{21}|^2 q_2$ and $|T_{22}|^2 q_2$ curves of the *Chiral* model, as given by Hyodo and Weise [15] as well as those of the *AY* model, are shown in Fig. 1 (upper) of Ref. [18]. They will be compared with the new HADES data at the end of the present paper.

C. Spectral function in pp reaction: $S(x)$

Now, we consider the spectrum function of the invariant mass, $S(x)$, in the case of pp reactions. We compose it by the incident channel, W_{form}(x), and the decay channel, $G(x)$, as follows:

$$S(x) = W_{\mathrm{form}}(x) \times G(x), \tag{II.6}$$

with

$$x = M(\Sigma\pi). \tag{II.7}$$

$G(x)$ is expressed in terms of the T matrices, T_{22} and T_{21}, as shown in Fig. 1 (a), (b). Each function calculated for an assumed M of the Λ^* pole is shown in Fig. 3.

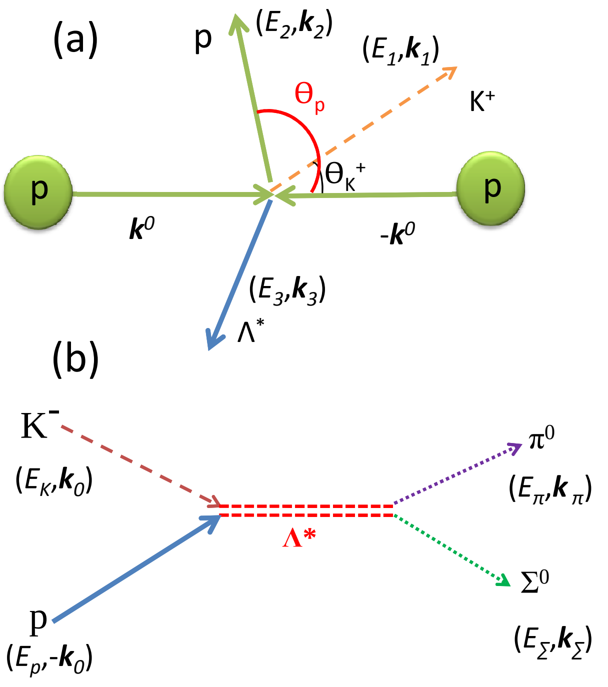

FIG. 2: (Color online) Kinematical variables in the center of mass of the $p+p$ collision for (a) the formation process, $W_{\rm form}$, and (b) the decay channel, $G(x)$.

D. Formation process function: $W_{\rm form}$

The Λ^* formation probability in a pp collision using the T-matrix is given as follows:

$$W_{\rm form}(x) = \frac{2|T_0|^2}{(2\pi)^3(\hbar c)^6}\frac{E_0}{k_0} \times \int dE_1 \int d\Omega_1\, d\Omega_2 (\frac{1}{1+b^2Q^2})^2 \times k_1k_2E_1E_2 \left[1+\frac{E_2}{E_3}(1+\frac{k_1}{k_2}\cos(\theta_{pK^+})\right]^{-1}, \quad \text{(II.8)}$$

where E_0 and k_0 are the initial energy and momentum in the c. m. frame, as given by

$$k_0 = \frac{1}{\hbar}\,[\frac{1}{2}M_p\, T_p]^{\frac{1}{2}}. \quad \text{(II.9)}$$

Also, $\theta_{pK^+} = (\theta_p - \theta_{K^+})$ is the angle between K^+ and p, b is the range of the $p-p$ reaction, and the momentum transfer, Q, is

$$Q = [{k_0}^2 + {k_2}^2 - 2\, k_0\, k_2 \cos\theta_{\rm p}]^{\frac{1}{2}}. \quad \text{(II.10)}$$

As can be seen from the factor, $1/(1+b^2Q^2)^2$, a shorter range of b can effectively moderate the strong suppression due to a large momentum transfer, Q, in a high-energy pp collision.

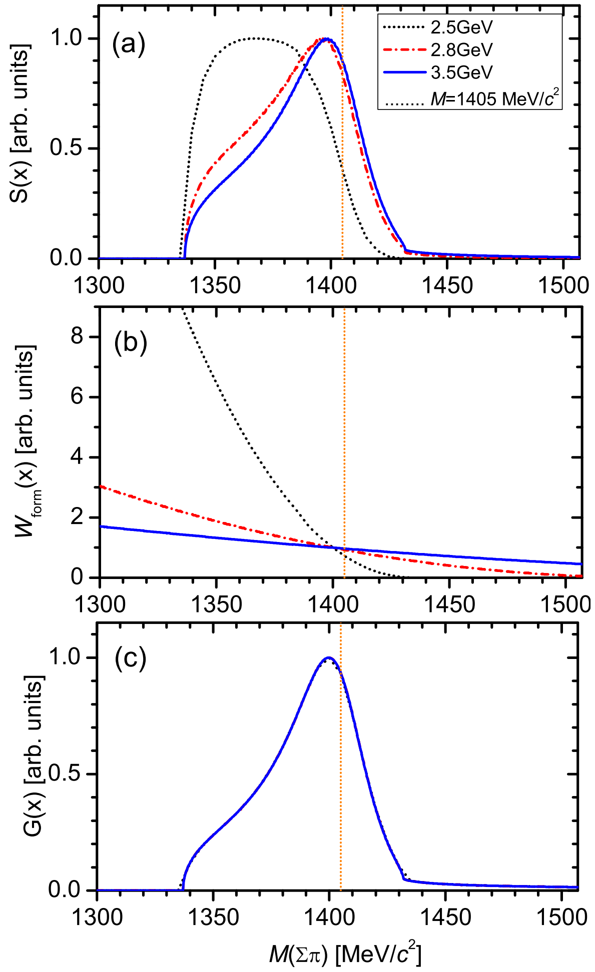

FIG. 3: (Color online) Normalized spectral functions $S(x)$ (a) composed of the formation-process function $W_{\rm form}$ (b) and the decay-process function $G(x)$ (c) for T_p = 2.50, 2.85 and 3.50 GeV. m_B = 770 MeV/c^2 and $(\theta_p, \theta_{pK^+})$ = (90,180). The M value of Λ^* is assumed to be 1405 MeV/c^2, as indicated by the vertical dashed line.

Figure 3 (b) shows the behavior of $W_{\rm form}(x)$ for T_p = 2.50, 2.83 and 3.50 GeV, which are normalized at x = 1400 MeV/c^2. They have respective kinematical upper limits, and make the mass distribution damp toward the kinematical limit. As a result, the observed spectrum shape, $S(x)$, changes, as demonstrated in Fig. 3 (a), whereas $G(x)$ is independent of T_p.

E. Decay process function: $G(x)$

The decay rate of $\Lambda(1405)$ to $(\Sigma\pi)^0$ is calculated by taking into account the emitted Σ and π particles realistically, following the generalized optical potential formalism in Feshbach theory [31], given by Akaishi *et al.* [5, 28]. The decay function, $G(x)$, is not simply a Lorentzian, but is skewed because the kinematic freedom of the decay particles is limited, particularly, when the incident proton energy, T_p, decreases and approaches the

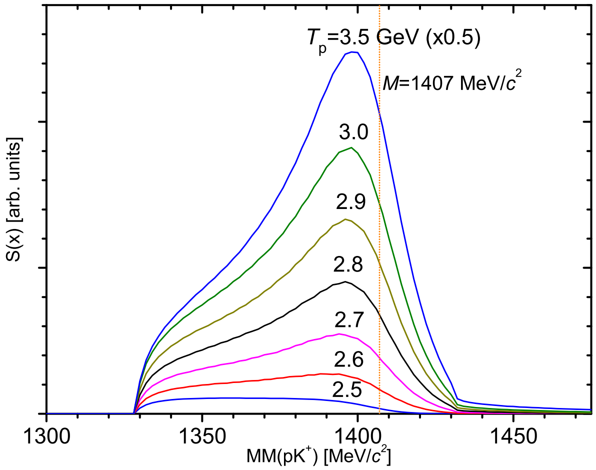

FIG. 4: (Color online) Incident energy dependence of the absolute values of the spectral function at m_B = 770 MeV/c^2 and $(\theta_p, \theta_{pK^+})$ = (90,180).

production threshold. Its general form is given as

$$G(x) = \frac{2(2\pi)^5}{\hbar^2 c^2} \frac{E_\pi E_\Sigma}{E_\pi + E_\Sigma} \text{ Re } [\tilde{k}(x)] \\ \times \left| \langle \tilde{k}(x) | t | \tilde{k_0}(x) \rangle \right|^2, \tag{II.11}$$

where the relative momenta in the entrance and exit channels of Fig. 2 (b) are calculated by:

$$\tilde{k_0}(x) = \frac{c\sqrt{\lambda(x, m_K, M_p)}}{2\,\hbar\, x} \tag{II.12}$$

and

$$\tilde{k}(x) = \frac{c\sqrt{\lambda(x, m_\pi, M_\Sigma)}}{2\,\hbar\, x} \tag{II.13}$$

with

$$\lambda(x, m_1, m_2) \equiv (x + m_1 + m_2)(x + m_1 - m_2) \\ \times (x - m_1 + m_2)(x - m_1 - m_2). \tag{II.14}$$

It should be noticed that $\lambda(x, m_K, M_p)$ becomes negative at around $x = 1400$ MeV/c^2, where we must choose a positive Im $\tilde{k}$ on the physical Riemann sheet. This case corresponds to direct excitation of the Λ^* quasi-bound state from the $p+p$ channel.

In the case of AY, the $T-$matrix is

$$\langle \tilde{k} | t_{21} | \tilde{k_0} \rangle = g(\tilde{k})\; T_{21}\; g(\tilde{k_0}) \tag{II.15}$$

for the T_{21} channel, and

$$g(\tilde{k}) = \frac{\Lambda^2}{\Lambda^2 + \tilde{k}^2} \tag{II.16}$$

with $\Lambda = m_B c/\hbar$, m_B being the mass of an exchanged boson, and $\tilde{k}$ is the relative momentum of Σ and π.

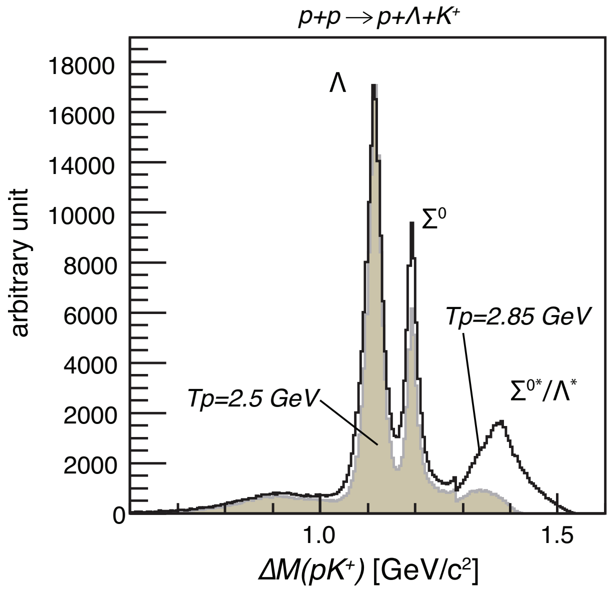

FIG. 5: (Color online) Experimental spectra of $\Delta M(pK^+)$ in the $pp \to p\Lambda K^+$ reaction at T_p = 2.50 and 2.85 GeV in DISTO experiments. Taken from [33].

The shape of $G(x)$, as given by eq.(II.11), includes the momenta, $\tilde{k_0}$ and $\tilde{k}$, which are functions of T_p. However, the function $G(x)$ is shown to depend only on the invariant-mass x, namely, $G(x)$ is a unique function of x and does not depend on T_p. It is bounded by the lower end $(M_l = M_\Sigma + m_\pi)$ = 1328 MeV/c^2) and the upper end $(M_u = M_p + m_{K^-})$ = 1432 MeV/c^2).

It is to be noted that the position of the peak in $G(x)$ is significantly lower than the position of the pole (M = 1405 MeV/c^2) in T_{21}, as assumed here and indicated by the vertical dashed line. Furthermore, the position of the peak (or centroid) of $S(x)$ is lowered due to the formation channel function $W_{\text{form}}(x)$.

III. NUMERICAL RESULTS

In this section we present results from numerical calculations, and discuss their physical implications. The importance of the present work is to consider both $W_{\text{form}}(x)$ and $G(x)$ functions. In most illustrative samples, we applied the AY model with the PDG parameters of [7], M =1407 MeV/c^2 and Γ = 50 MeV. To compare the *Chiral* model with the AY model on equal footing, we also applied the same procedure as above to Hyodo-Weise's T-matrices to obtain realistic spectrum shapes $S(x)$.

A. Dependence on the incident energy, T_p

Regarding eqs.(II.6, II.8, II.11) again, it is clear that the spectral function depends on the incident proton energy due to the $W_{\rm form}(x)$ function and $G(x)$. Figure 4 shows absolute values of spectral functions $S(x)$ for various incident energies (T_p) at m_B = 770 MeV/c^2 and $(\theta_p, \theta_{pK^+})$ = (90,180). The shape of $S(x)$ is nearly the same, but toward the reaction threshold ($T_p^{\rm thresh} = 2.42$ GeV) not only the absolute value diminishes, but also the spectral shape changes drastically, as shown in Fig. 3(a) for the normalized spectral functions at T_p =3.50, 2.83, 2.50 GeV. The most extreme case is seen at $T_p = 2.50$ GeV, where the main part of $x > 1400$ MeV/c^2 is missing due to the kinematical constraint, and a very skewed component below 1400 MeV/c^2 appears.

B. Behavior near the production threshold of T_p

The above prediction is indeed in good agreement with the observed spectra of DISTO at $T_p = 2.50$ and 2.85 GeV [33], as shown in Fig. 5. Even in such a very skewed spectrum, one can extract the decay function, $G(x)$, from an observed spectral function by taking the ratio

$$DEV[G(x)] \equiv \frac{S(x)^{\rm obs}}{W_{\rm form}(x)} \qquad \text{(III.17)}$$

using a calculated $W_{\rm form}$ function. This is a kind of the *deviation spectrum method* introduced in stopped-K^- spectroscopy [18].

C. Angular distribution and correlation

The cross section of this reaction has substantial angular dependence (Fig. 7), but the bound-state peak is distinct at any angle, and we can choose $(\theta_p, \theta_{pK^+}) = (90, 180)$, because the cross section is modest and the peak-to-background ratio remains large. The normalized cross sections (spectral shapes) at various angles are found to be nearly the same. Since the two incident protons are indistinguishable, the $\Lambda(1405)$ formation process is angular symmetric, as shown in Fig. 7. We can write

$$\sigma_S(\theta_p, \theta_{pK^+}) = \sigma_S(\pi - \theta_p, -\theta_{pK^+}) \qquad \text{(III.18)}$$

for $\theta_p = 0 - 90^\circ$ and $\theta_{pK^+} = 0 - 180^\circ$.

According to eq. (II.8) and eq. (II.10), $W_{\rm form}$, and thus the spectral function, $S(x)$, are related to the outgoing proton angle, θ_p, and the angle between the outgoing proton and K^+, θ_{pK^+}, as shown in Fig. 6. Although these curves look different, the spectrum shape does not depend on the angle. We choose and use $\theta_p = 90^\circ$, $\theta_{pK^+} = 180^\circ$ in all of the following calculations.

D. Dependence on the exchanged boson mass

Figure 7 shows the normalized angular distributions of the outgoing proton, θ_p, for various masses of the exchanged boson, m_B = 2000, 770 and 140 MeV/c^2, at

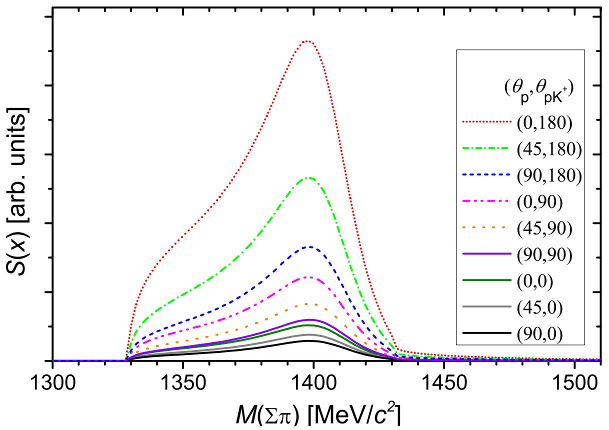

FIG. 6: (Color online) The spectral functions for various angles, $(\theta_p,\ \theta_{pK^+})$, for T_p = 3.50GeV and m_B=770 MeV/c^2.

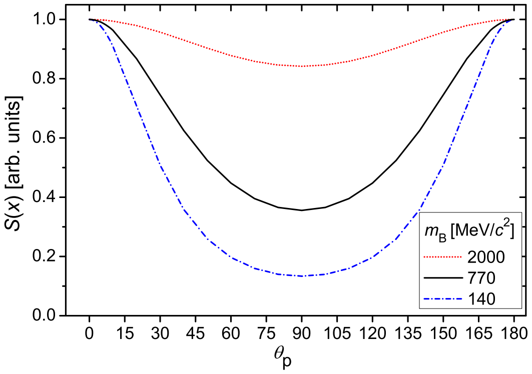

FIG. 7: (Color online) Normalized angular distributions of the outgoing proton for different exchanged boson masses, m_B = 2000, 770 and 140 MeV/c^2 at T_p = 3.50GeV.

T_p = 3.50GeV. The nearly isotropic angular distribution with a large boson mass explains the experimental data of HADES at T_p = 3.50 GeV [29, 30], which shows that the proton angular distributions together with $\Lambda(1405)$ and $\Lambda(1520)$ are nearly isotropic. A similar behavior is observed in the DISTO data at T_p = 2.85 GeV (see Fig. 5 [33, 34]). Such a short collision length as revealed in the production of $\Lambda(1405)$ in the *pp* reaction is one of the key mechanisms (Λ^* doorway) responsible for forming K^-pp from high sticking of Λ^* and p [4]. On the other hand, it is well known that the proton emitted in the ordinary $pp \to p + \Lambda + K^+$ reaction has sharp forward and backward distributions, indicating that the mediating boson is $m_B = m_\pi$ [32–34].

IV. χ^2 FITTING OF HADES DATA

In this section we analyze the recent HADES data for charged final states of $\Sigma^-\pi^+$ and $\Sigma^+\pi^-$ in a *pp* collision at T_p = 3.50 GeV. The data we use are the missing-mass spectra, $MM(pK^+)$, deduced by the HADES group, as

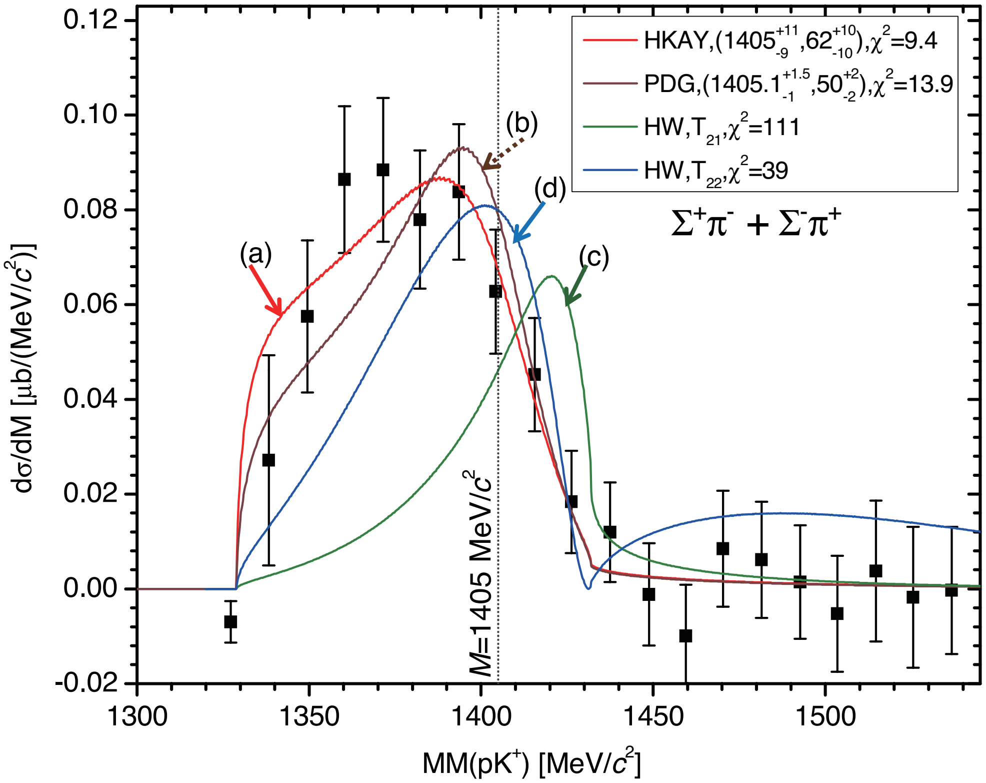

FIG. 8: (Color online) Comparison of HADES data ($\Sigma^+\pi^- + \Sigma^-\pi^+$, closed squares) at $T_p = 3.50$ GeV [30] with best-fit theoretical spectral functions $S(x)$. a) Best-fit HKAY curves (with $\chi^2 = 9.5$, $M = 1405^{+11}_{-9}$ MeV/c^2 and $\Gamma = 62 \pm 10$ MeV). b) AY model with the PDG parameters (with $\chi^2 = 14$, $M = 1405.1^{+1.3}_{-1.0}$ MeV/c^2 and $\Gamma = 50$ MeV [8]). The *Chiral* model using HW's T_{21} (with $\chi^2 = 111$, c)) and T_{22} (with $\chi^2 = 40$, d)).

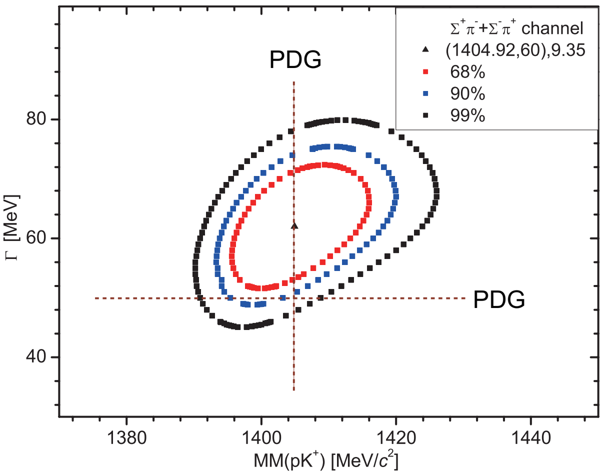

FIG. 9: (Color online) Confidence level contours from χ^2 fitting of the HADES data of $\Sigma^+\pi^- + \Sigma^-\pi^+$ at $T_p = 3.50$ GeV. The PDG values are also shown.

given in Fig. 1 of [30], which are corrected for acceptance and efficiency of the detector system. They are expressed as

$$Y(x) = Y_{\Lambda^*}(x) + Y_{\Sigma^*}(x) + Y_{\Lambda 1520}(x) + Y_{\rm NonRes}(x), \tag{IV.19}$$

with Y_{Λ^*} for Λ^*, Y_{Σ^*} for $\Sigma(1385)$, $Y_{\Lambda 1520}$ for $\Lambda(1520)$, and $Y_{\rm NonRes}$ for non-resonant continuum. They decomposed the experimental data, $Y(x)$, by the above four components, which were obtained by model simulations, among which the $\Sigma(1385)$ and the $\Lambda(1520)$ components were determined by using the experimental data. The shape of the non-resonant $\Sigma\pi$ continuum was simulated. In their fitting they cautiously excluded the area around 1400 MeV/c^2 for $MM(pK^+)$ in order not to bias the finally extracted shape of the Λ^* resonance. Then, they found that a simulation of the Λ^* region by using a relativistic s-wave Breit-Wigner distribution with a width of 50 MeV/c^2 and a pole mass of 1385 MeV/c^2 can reproduce the experimental data very well, but using instead the nominal mass of 1405 MeV/c^2 fails.

This conclusion depends on their assumption of the symmetric Breit-Wigner shape, which is not valid in the case of a broad resonance with adjacent endpoints, $M(\Sigma + \pi)$ and $M(p + K^-)$, as we have seen. Thus, in turn, we decided to set up an excess component, $Y_{\Lambda^*}(x)$, by subtracting the given three components from the experimental spectrum $Y(x)$ as

$$Y_{\Lambda^*}(x) = Y(x) - Y_{\Sigma^*}(x) - Y_{\Lambda 1520}(x) - Y_{\rm NonRes}(x), \qquad \text{(IV.20)}$$

where the statistical errors of $Y(x)$ are inherited to $Y_{\Lambda^*}(x)$.

The HADES spectra, as given in Fig. 1 of [30], indicate that the spectra of both charged channels are similar to each other, yielding nearly the same M values. This fact indicates that the $\Sigma\pi$ resonance is formed by nearly pure charged states, $\Sigma^+\pi^-$ and $\Sigma^-\pi^+$, without isospin mixing. It also justifies the use of T_{21} for the analysis of $M(\Sigma\pi)$ in the case of pp reactions. On the other hand, the statistical fluctuation of each charged-channel spectrum is rather large. Thus, for the final analysis we use the sum data of HADES ($\Sigma^+\pi^- + \Sigma^-\pi^+$), which is presented in Fig. 1(c) of [30]. Keeping the last three components of eq. (IV.20) fixed, we fit the experimental data of $Y_{\Lambda^*}(x)$ with n =21 data points in the range of 1300 to 1550 MeV/c^2 (closed points with error bars in Fig. 8) by assumed theoretical functions $S(x)$.

Generally, the experimental histogram, N_i, i= 1, ..., n with respective statistical errors, σ_i, is fitted to a theoretical curve, $S(x; M, \Gamma)$ with $x = MM(pK^+)$ involving the mass M and width Γ as free parameters by minimizing the χ^2 value:

$$\chi^2(M,\Gamma) = \sum_{i=1}^{n} \left(\frac{N_i - S(x_i; M, \Gamma)}{\sigma_i} \right)^2 . \qquad \text{(IV.21)}$$

Figure 8 shows the results of the χ^2 fitting, where the HADES data ($\Sigma^+\pi^- + \Sigma^-\pi^+$) at T_p = 3.50 GeV [30] are compared with best-fit theoretical spectral functions, $S(x)$. The present AY treatment (hereafter, called HKAY), adopting the PDG values ($M = 1405.1^{+1.3}_{-1.0}$ MeV/c^2 and $G = 50$ MeV [8]), gives a remarkable fitting with $\chi^2 = 11$, which is comparable with the statistically expected value, $< \chi^2 >_{\rm exp} \sim 19$. On the other hand, the *Chiral* model gives much larger χ^2 values of ~ 111, when T_{21} is chosen, and of 39, when T_{22} is chosen. Another *Chiral* model spectrum by Geng and Oset [26] is almost identical to HW's T_{21}. Thus, the chiral models indicate a substantial deviation from the experimental data.

Furthermore, we can find best-fit values of (M, Γ) from drawing confidence contour curves by varying the parameters, (M, Γ) in a plane. The results are shown in Fig. 9. From this contour mapping we obtain the following best-fit values with 68% CL (1σ) errors:

$$M = 1405^{+11}_{-9}\ {\rm MeV}/c^2, \qquad \text{(IV.22)}$$

$$\Gamma = 62 \pm 10\ {\rm MeV}. \qquad \text{(IV.23)}$$

The best-fit curves are shown together with the experimental points in Fig. 8. The M value thus obtained from the present analysis of the new HADES data confirms the traditional value [7, 8].

V. CONCLUDING REMARKS

We have presented results of our calculation for the spectral shape of $MM(pK^+)$ in the $pp \to p\Lambda^* K^+$ reaction based on the $\bar{K}N$-$\Sigma\pi$ coupled-channel treatment. We took into account both the entrance process and the decay process. The formation probability, $W_{\rm form}$, of Λ^* in a pp collision and the decay rate, $G(x)$ to $(\Sigma\pi)^0$, were formulated. The spectral function is given by $S(x) = W_{\rm form} \times G(x)$. It was found to be asymmetric and skewed due to the kinematic limitation imposed by the entrance channel. The peak of $S(x)$ is not located at the pole position.

With this tool in hand we analyzed the recent HADES data. Although the observed spectra of $MM(pK^+)$ appear to show the peak position at around 1385 MeV/c^2, the χ^2 fitting by our theoretical spectral functions provided $M = 1405^{+11}_{-9}$ MeV/c^2. This value is in good agreement with the values obtained from a recent analysis [17] of an old experimental data of stopped-K^- in ^{4}He [19], taken up as the updated PDG value ($M = 1405.1^{+1.3}_{-1.0}$) [8]. On the other hand, the *Chiral* model with $M \sim 1420$ MeV/c^2 cannot reproduce the experimental data.

The proton angular distribution in the Λ^* production was also calculated. The isotropic distribution observed in HADES [30] and DISTO [33, 34] were explained by a short-range collision with an intermediate boson mass heavier than the ρ meson mass. This is consistent with the calculated large cross section for the production of K^-pp in pp collisions [4], which has recently been observed in DISTO experiments [32].

VI. ACKNOWLEDGMENTS

This work is supported by a Grant-in-Aid for Scientific Research of Ministry of Science, Research, and Technology of Iran and by a Grant-in-Aid for Scientific Research of Monbu-Kagakusho of Japan. One of us (T.Y.) acknowledges support by an Award of the Alexander von Humboldt Foundation, Germany.

---

[1] M.H. Alston *et al.*, Phys. Rev. Lett. **6**, 698 (1961).
[2] R.H. Dalitz and S.F. Tuan, Ann. Phys. **8**, 100 (1959).
[3] Y. Akaishi and T. Yamazaki, Phys. Rev. **C 65**, 044005 (2002).
[4] T. Yamazaki and Y. Akaishi, Phys. Rev. **76**, 045201 (2007).

[5] Y. Akaishi, K. S. Myint and T. Yamazaki, Proc. Jpn. Acad. **B 84**, 264 (2008).

[6] R.H. Dalitz and A. Deloff, J. Phys. G: Nucl. Part. Phys. **17**, 289 (1991).

[7] Particle Data Group, K. Nakamura *et al.*, J. Phys. **G 37**, 075021 (2010).

[8] Particle Data Group, J. Beringer *et al.*, Phys. Rev. **D 86**, 010001 (2012).

[9] T. Yamazaki and Y. Akaishi, Phys. Lett. **B 535**, 70 (2002).

[10] A. Doté, H. Horiuchi, Y. Akaishi and T. Yamazaki, Phys. Lett. **B 590**, 51 (2004).

[11] A. Doté, H. Horiuchi, Y. Akaishi and T. Yamazaki, Phys. Rev. **C 70**, 044313 (2004).

[12] T. Yamazaki, A. Doté, Y. Akaishi, Phys. Lett. **B 587**, 167 (2004).

[13] D. Jido, J.A. Oller, E. Oset, A. Ramos and U.G. Meissner, Nucl. Phys. **A 725**, 181 (2003).

[14] V. K. Magas, E. Oset and A. Ramos, Phys. Rev. Lett. **95**, 052301 (2005).

[15] T. Hyodo and W. Weise, Phys. Rev. **C 77**, 035204 (2008).

[16] A. Doté, T. Hyodo and W. Weise, Phys. Rev. **C 79**, 014003 (2009).

[17] J. Esmaili, Y. Akaishi and T. Yamazaki, Phys. Lett. **B 686**, 23 (2010).

[18] J. Esmaili, Y. Akaishi and T. Yamazaki, Phys. Rev. **C 83**, 055207 (2011).

[19] B. Riley, I-T. Wang, J.G. Fetkovich and J.M. McKenzie, Phys. Rev. **D 11**, 3065 (1975).

[20] T. Suzuki, J. Esmaili and Y. Akaishi, EPJ Web Conf. **3**, 07014 (2010).

[21] D. Jido, E. Oset and T. Sekihara, Eur. Phys. J. **A 42**, 257 (2009).

[22] K. Miyagawa and J. Haidenbauer, arXiv:1202.4272 [nucl-th].

[23] O. Braun *et al.*, Nucl. Phys. **B 129**, 1 (1977).

[24] J-PARC E31 experiment (2012).

[25] I. Zychor *et al.*, Phys. Lett. **B 660**, 167 (2008).

[26] L. S. Geng and E. Oset, Eur. Phys. J. **A 34**, 405 (2007).

[27] R.J. Hemingway, Nucl Phys. **B 253**, 742 (1985).

[28] Y. Akaishi, T. Yamazaki, M. Obu and M. Wada, Nucl., Phys. **A 835**, 67 (2010).

[29] G. Agakishiev *et al.* (HADES collaboration), Nucl. Phys. **A 881**, 178 (2012).

[30] G. Agakishiev *et al.* (HADES collaboration), arXiv:1208.0205v1 [nucl-ex](2012).

[31] H. Feshbach, Ann. Phys. **5**, 357 (1958); **19**, 287 (1962).

[32] T. Yamazaki *et al.*, Phys. Rev. Lett. **104**, 132502 (2010).

[33] P. Kienle *et al.*, arXiv:1102.0482v2 [nucl-ex].

[34] K. Suzuki *et al.*, to be published (2012).